

# Rotor dynamics analysis and experiment study of the flywheel spin test system<sup>†</sup>

Chang-Liang Tang<sup>\*</sup>, Xing-Jian Dai, Xiao-Zhang Zhang and Lei Jiang

*Department of Engineering Physics, Tsinghua University, Beijing 100084, China*

(Manuscript Received November 3, 2011; Revised February 25, 2012; Accepted March 23, 2012)

## Abstract

The strength study of the flywheel is important to the flywheel energy storage. The motor and bearing are the key challenges for the high-speed flywheel spin test device in vacuum. By using a small stiffness pivot-jewel bearing and a spring squeeze film damper as the lower support of the flywheel, a simple spin system was designed at a low cost and is suitable for longtime operation. The auxiliary support at the top was not removed until the flywheel passed the first critical speed. The flywheel that kept its rigid state in sub-critical state was tested at the high speed without the top support. The dynamic model of the flywheel-bearing-damper was built by means of the Lagrangian equation to calculate critical speeds, mode shapes and modal damping ratios at different speeds. The lower damper's effects on the modal damping ratios and forced vibration were discussed. The vibrations of the flywheel-bearing-damper system were measured at the different damping coefficients in the experiment. When the lower damper was adjusted to be overdamped, the flywheel ran up to 50000 r/min steadily, and the experimental result was in agreement with the theoretical assumption. The sub-critical rotor dynamics design and pivot-jewel bearing proved to be good solutions to the spin test for the composite flywheel.

*Keywords:* Spin test; Critical speed; Mode shape; Modal damping ratio; Stability; Overdamped

## 1. Introduction

In a flywheel energy storage system, the excess electrical energy is stored as kinetic energy of a rotating flywheel rotor and is converted to electrical energy when needed. The rise and fall of the rotating speed of the flywheel realizes the storage and release of the electrical energy [1, 2], which has high energy density, high efficiency and high power density. The design life has no degradation during its entire cycle life, unlike chemical batteries. Current testing indicates that flywheels are not damaged by repetitive very deep discharge. It can be widely applied to space satellites of low earth orbits, launch vehicles, uninterruptable power supplies, pulse power transfer for hybrid electric vehicles and prevent instantaneous voltage change, smoothing wind power output and so on [3–8].

The flywheel energy density (kinetic energy stored in per flywheel mass) is an important index of evaluating the flywheel structure design. The kinetic energy stored in a flywheel is proportional to the square of its speed, which is mostly limited by the strengths of the materials and structure centrifugal stress. To increase the energy density, high strength and lightweight composite materials are used for manufacturing the flywheel rotor besides optimizing its structure. However, the transverse strength of the filament wound flywheel is

much lower than the hoop one, which makes each ring of the rotor separate at rotation easily. Many scholars have done extensive work on the strength theory and design of the composite flywheel [9–12]. To improve the energy density, multi-ring pressfit is developed and proven to be one effective way of solving the problem that the radial strength of composite flywheel is too low, and the method of tension winding of fiber bundle is also used to reduce the radial stress. The finite element method is for optimizing the flywheel structure with complex shape. However, their investigations are limited to theoretical analyses and calculations, and short of spin tests. There is little research on the developments and dynamic analyses of the high speed spin test system, which is mainly because of great difficulty in vacuum technology, motor technology and bearing technology. The tangential velocity of the advanced composite flywheel is at least more than 600 m/s, at which the flywheel must be enclosed in a high vacuum to reduce friction and energy losses. Centrifugal load generated by high speed are also a huge challenge to the technology of a driven motor, as the rotating speed of motor is limited by its material strength and the performance of heat dissipation of stator. The output power of the motor whose rated speed is over 40000 r/m is usually about several kilowatts. To test the structural fatigue life, the flywheel needs to be in continuous operation at high speed, which is over 40000 r/m. The service life of conventional bearings is reduced considerably when in ultra-high-speed operation, and the friction loss is usually

<sup>\*</sup>Corresponding author. Tel.: +86 10 62784518, Fax.: +82 10 62782658

E-mail address: tangle08@mails.tsinghua.edu.cn

<sup>†</sup>Recommended by Associate Editor Jun Sik Kim

greater than the output power of the motor, which cannot meet the requirements of a high speed spin test. The mechanical investigations of a composite flywheel are limited to theoretical analyses and calculations for these reasons above.

The strength study of the flywheel is an important part for the technology of flywheel energy storage. The Electrical Research Center at the University of Texas at Austin had performed a composite flywheel burst test. Professor Bakis's research team at Pennsylvania State University used a 70000 r/m hydraulic turbine to drive a flywheel in the vacuum chamber. The maximum tangential test velocity was 1100 m/s. The FESS prototype II developed by Flywheel Laboratory at Tsinghua University was up to full speed 42000 r/m, corresponding to tangential velocity 660 m/s in many charge-discharge cycles. However, the turbine-driven spin test has low efficiency, high cost, difficulties in adjustable speed and disagreement of lasting fatigue strength test. Because the flywheel energy storage system is developed by high cost and has complex structure, strength failure of the flywheel can destroy the whole system.

To do the flywheel spin test efficiently, it is necessary to establish a spin test system which is stable, simple, and easy to regulate speed and suitable for longtime operation. For the spin test, the flywheel-bearing-damper system generally uses the super-critical rotor dynamic design. However, the flywheel rotor keeps its rigid state in sub-critical. For the rigid rotor in sub-critical operation, the rotor-bearing system does not have the second-order critical speed if the flywheel inertia ratio  $J_d/J_p$  is less than 0.8. The rotor only passes through a first-order one. The dampers with appropriate parameters enhanced the stability of the rotor-bearing system and made the system run to rated speed smoothly [13, 14].

Based on the dynamics theory of super-critical operation above, we designed and established a flywheel spin test system (as shown in Fig. 1), which used a small stiffness pivot-jewel bearing [15, 16] and a spring squeeze film damper as its lower support but no upper support. The system has simple structure and very low cost. By means of the Lagrangian equation, a dynamic model of the vertical flywheel-bearing-damper was built to calculate critical speeds, mode shapes and modal damping ratios at different speeds. The function of the lower damper and its effects on the modal damping ratios and forced vibration were discussed. The vibrations of the flywheel-bearing-damper system were measured at the different damping coefficients in the experiment. The results provide a reliable theoretical basis for optimization and improvement of the spin test system, and are helpful to develop strength research of a composite flywheel more efficiently.

## 2. Dynamic model of the spin test system

### 2.1 Spin test system and its dynamic simplified model

Fig. 1 shows a schematic of the flywheel-bearing-damper system, which is installed in a high vacuum steel container. The flywheel is integrated with the rotor of a disk type motor,

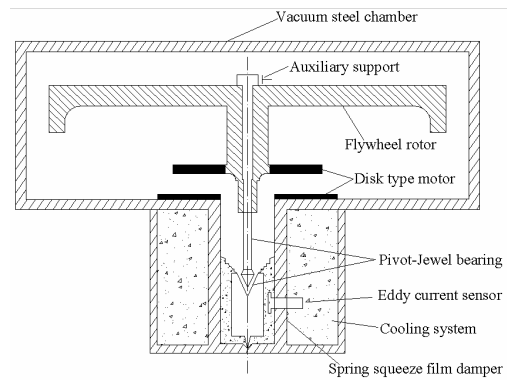


Fig. 1. The flywheel-bearing-damper system.

so that the structure is simple and efficient. Compared with a conventional motor, the disk type motor has smaller volume, and its stator uses the same cooling system with the lower damper. The bottom of the flywheel is supported by a jewel-bearing with a very flexible small pivot.

The pivot-jewel bearing is lubricated by vacuum pump oil. The section diameter of the pivot is about 2 mm, and the contact area between pivot and jewel bearing is about  $1.5 \text{ mm}^2$ , so the friction loss is very small, which makes the motor work efficiently. The service life of the pivot-jewel bearing is over 10000 hours in super high vacuum environments. The jewel bearing is fixed on the damping body, which connects the outer shell by three small stiffness springs. The springs can also provide radial stiffness for the damper. The squeeze oil film in the damper that provides damping suppresses the vibration of the damping body and ensures that the jewel bearing works well. There is no oil feed cycle system for the pivot-jewel bearing and the spring squeeze film damper. The friction heat of the lubricating oil is conducted to the cooling system of the disk type motor through the housing of the damper.

The lower damper, which is a key component of the flywheel-bearing system, is simplified to a spring-oscillator model with a single degree of freedom on the basis of its working principle. The response of the damper is checked by the eddy current sensor under excess excitation. According to vibration theory of a single degree of freedom, the equivalent mass, the equivalent stiffness and the equivalent damping coefficient of the lower damper can be obtained.

The dynamic model is illustrated in Fig. 2. It should be pointed out that the vibration displacements in the  $x$  and  $y$  directions compose the complex vibration displacement of  $r$  ( $r = x + iy$ ).

In linear modeling, the following simplifications are made: (1) The lateral vibration is small and considered as linear. (2) The flywheel is rigid. (3) The stiffness of boundary oil film in the pivot-jewel bearing is much higher than that of the pivot. Therefore, the lower end of the pivot is fixed to the jewel bearing. (4) The small pivot with much flexibility and infinitesimal mass acts as elastic element connecting the flywheel with jewel bearing, so the pivot is equivalent to a spring without

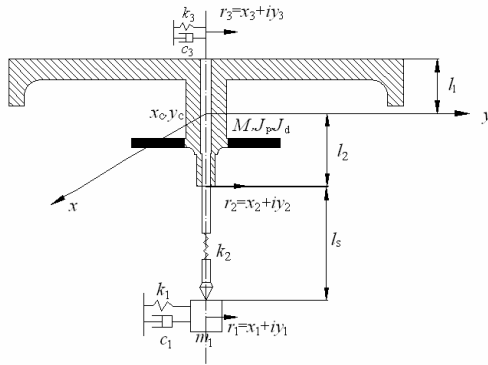


Fig. 2. The dynamic model.

mass. (5) The action of the oil in the damper is described by a linear stiffness and damping coefficient. The symbols in Fig. 2 are described in the nomenclature.

**2.2 The dynamic equations of the flywheel system**

For the dynamic model shown in Fig. 2, based on Lagrangian method, the kinetic energy function  $T_i$ , the potential energy function  $U_i$ , and the consumed energy function  $Z_i$  were written as follows:

(1) The spring squeeze film damper

$$\begin{aligned} T_1 &= \frac{1}{2} m_1 (\dot{x}_1^2 + \dot{y}_1^2), \\ U_1 &= \frac{1}{2} k_1 (x_1^2 + y_1^2), \\ Z_1 &= \frac{1}{2} c_1 (\dot{x}_1^2 + \dot{y}_1^2). \end{aligned} \tag{1}$$

(2) The pivot is equivalent to a spring without mass

$$\begin{aligned} U_{12} &= \frac{1}{2} k_2 \left\{ \left[ (x_2 - x_1) - \frac{l_3}{l} (x_3 - x_2) \right]^2 \right. \\ &\quad \left. + \left[ (y_2 - y_1) - \frac{l_3}{l} (y_3 - y_2) \right]^2 \right\}. \end{aligned} \tag{2}$$

(3) The flywheel

$$\begin{aligned} T_2 &= \frac{1}{2} M (\dot{x}_c^2 + \dot{y}_c^2) + \frac{1}{2} J_p \omega (\omega + 2\dot{\alpha}\beta) \\ &\quad + \frac{1}{2} J (\dot{\alpha}^2 + \dot{\beta}^2) \end{aligned} \tag{3}$$

where

$$\begin{aligned} x_c &= \frac{l_2 x_3 + l_1 x_2}{l}, y_c = \frac{l_2 y_3 + l_1 y_2}{l} \\ \alpha &= \frac{x_3 - x_2}{l}, \beta = \frac{y_3 - y_2}{l}. \end{aligned}$$

(4) The auxiliary support

$$\begin{aligned} U_3 &= \frac{1}{2} k_3 (x_3^2 + y_3^2), \\ Z_3 &= \frac{1}{2} c_3 (\dot{x}_3^2 + \dot{y}_3^2). \end{aligned} \tag{4}$$

Therefore, the kinetic energy of the flywheel-bearing-damper system is  $T = T_1 + T_2$ . The potential energy of the flywheel-bearing-damper system is  $U = U_1 + U_{12} + U_3$ . The consumed energy of the flywheel-bearing-damper system is  $Z = Z_1 + Z_2$ . By means of the Lagrange equation

$$\frac{d}{dt} \left( \frac{\partial T}{\partial \dot{q}_i} \right) - \frac{\partial T}{\partial q_i} + \frac{\partial U}{\partial q_i} + \frac{\partial Z}{\partial q_i} = \bar{Q}_i, \text{ when } \bar{Q}_i = 0, \text{ the free vibration equation of the flywheel-bearing-damper system was obtained and written in the matrix form:}$$

$$[M] \{\ddot{r}\} + ([C] - i\omega[H]) \{\dot{r}\} + [K] \{r\} = \{0\} \tag{5}$$

where

$$[M] = \begin{bmatrix} m_1 & 0 & 0 \\ 0 & m_2 & m_0 \\ 0 & m_0 & m_3 \end{bmatrix}, [C] = \begin{bmatrix} c_1 & 0 & 0 \\ 0 & 0 & 0 \\ 0 & 0 & c_3 \end{bmatrix},$$

$$[H] = \begin{bmatrix} 0 & 0 & 0 \\ 0 & \frac{J_p}{l^2} & -\frac{J_p}{l^2} \\ 0 & -\frac{J_p}{l^2} & \frac{J_p}{l^2} \end{bmatrix},$$

$$[K] = \begin{bmatrix} k_1 + k_2 & -\left(k_2 + \frac{k_2 l_s}{l}\right) & \frac{k_2 l_s}{l} \\ -\left(k_2 + \frac{k_2 l_s}{l}\right) & k_2 + \frac{k_2 l_s^2}{l^2} + \frac{2k_2 l_s}{l} & -\left(\frac{k_2 l_s^2}{l^2} + \frac{k_2 l_s}{l}\right) \\ \frac{k_2 l_s}{l} & -\left(\frac{k_2 l_s^2}{l^2} + \frac{k_2 l_s}{l}\right) & \frac{k_2 l_s^2}{l^2} + k_3 \end{bmatrix}.$$

$$m_2 = \frac{M l_1^2 + J_d}{l^2}, m_3 = \frac{M l_2^2 + J_d}{l^2}, m_0 = \frac{M l_1 l_2 - J_d}{l^2}, \{\ddot{r}\} \text{ and } \{\dot{r}\}$$

represent the second derivative and the first derivative of displacement column vector  $\{r\} = [r_1 \ r_2 \ r_3]$ , and  $r_j = x_j + iy_j, (j=1,2,3)$ . State vector method can be used to solve Eq. (5), whose solution form is

$$r_j = R_j e^{st}, (j=1,2,3). \tag{6}$$

The complex vibration amplitudes and complex frequencies are

$$R_j = X_j + iY_j, (j=1,2,3). \tag{7}$$

$$s = \lambda + i\omega$$

In which  $\lambda$  is the mode decaying exponent,  $\omega = 2\pi f$  is the mode angular frequency and  $f$  is the modal frequency. The modal damping ratio  $\zeta = -\frac{\lambda}{\omega}$ , and if  $\lambda > 0$ , the dynamic system is stable. The larger  $|\zeta|$  is, the better stability the system has. So the modal frequencies, mode shapes and modal damping ratios of the flywheel system were obtained by solving Eq. (5). In engineering practice, the flywheel rotor inevitably exists an unbalance; if the residual unbalance is  $\{f\} = \{u\} \omega^2 e^{i\omega t}$  at the flywheel rotor top, the forced vibration equation of the flywheel dynamic system is obtained by means of the Lagrangian equation:

$$[M]\{\ddot{r}\} + ([C] - i\omega[H])\{\dot{r}\} + [K]\{r\} = \{u\} \omega^2 e^{i\omega t}. \quad (8)$$

The steady state unbalance response was calculated from Eq. (8).

### 3. The dynamic simulation of the flywheel-bearing-damper system

Take a flywheel rotor in our laboratory as a research object. The parameters and corresponding values of the flywheel dynamic system are as follows:

$$\begin{aligned} m_1 &= 0.0197 \text{ kg}, \quad M = 0.591788 \text{ kg}, \quad J_p = 5.798e-4 \text{ kg}\cdot\text{m}^2, \\ J_d &= 4.092e-4 \text{ kg}\cdot\text{m}^2, \quad l = 66.1 \text{ mm}, \quad l_1 = 24.993 \text{ mm}, \\ l_2 &= 41.106 \text{ mm}, \quad l_3 = 26 \text{ mm}, \quad k_1 = 586.18 \text{ N/m}, \\ c_1 &= 0.2875 \text{ N}\cdot\text{s/m}, \quad k_2 = 5030 \text{ N/m}, \quad k_3 = 800 \text{ N/m}, \quad c_3 = 0 \text{ N}\cdot\text{s/m}. \end{aligned}$$

#### 3.1 Critical speeds

Fig. 3 shows the mode frequencies of the flywheel dynamic system with different speed, also known as the Campbell diagram. In Fig. 3, ‘1F’ and ‘1B’ indicate the first-order forward and backward whirl of the flywheel, respectively. ‘LDF’ and ‘LDB’ indicate the forward and backward whirl of the lower damper respectively. ‘2F’ and ‘2B’ indicate the second-order forward and backward whirl of the flywheel, respectively.

From the figure, we can see that the frequencies of the modes change over the speed range. The behavior is due to a gyroscopic effect that occurs whenever the mode shape has an angular component. The first-order and second-order modes of the flywheel split into forward and backward modes. The forward modes increase in frequency with increasing speed, while the backward modes decrease in frequency with increasing speed. How much the mode changes depends on the distribution of mass and diametral mass moment of inertial and the shape of the corresponding mode shape. In this case, the gyroscopic effect mainly affects the second-order modes of the flywheel. As rotating speed increases, the gyroscopic effect essentially acts like an increasingly stiff spring on the flywheel for the second-order forward whirl. For the second-order backward whirl, the effect is reversed. For the first-order

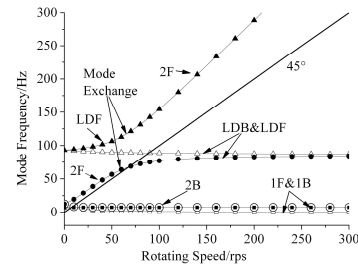


Fig. 3. Mode frequencies of the flywheel rotor dynamic system.

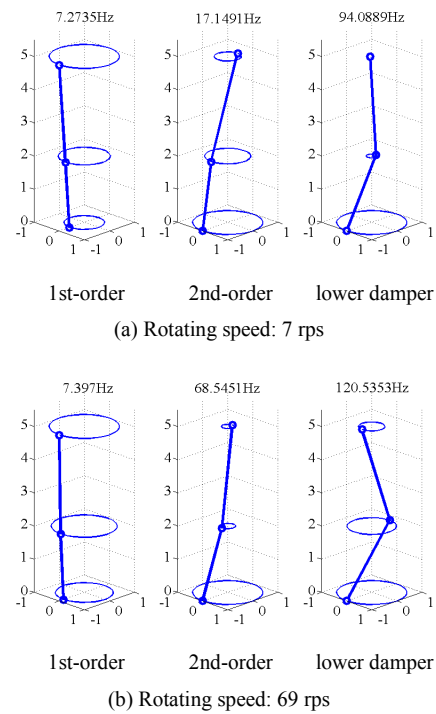


Fig. 4. Mode shapes of the flywheel dynamic system.

modes, the effect is small. It was found that the lower damper mode and conical mode of the flywheel rotor exchange for each other when in the speed range 80 rps~100 rps. The exchange of modes is completed when the rotating speed exceeds 100 rps (see Section 3.2). Critical speeds occur at the peak response speed when the forward whirl frequency is equal to the rotating frequency. For the dynamic system as shown in Fig. 2, the critical speeds are 7 rps (1<sup>st</sup> mode) and 69 rps (lower damper mode). It was found that the flexible pivot greatly decreases the critical speeds. There will be no critical speed when the flywheel passes the two critical speeds.

#### 3.2 Mode shapes

The mode shapes when the flywheel passes critical speeds are as shown in Fig. 4(a) and Fig. 4(b), respectively. Three hollow dots from top to bottom of the two figures represent coordinates of the flywheel rotor top, the flywheel rotor bottom and the lower damper, respectively.

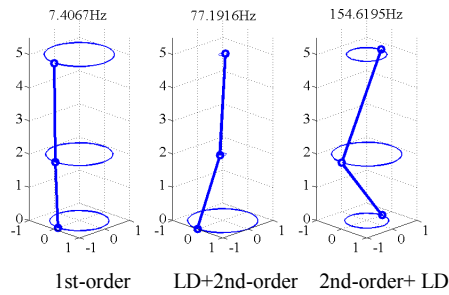


Fig. 5. Mode shapes (Rotating speed:100 rps).

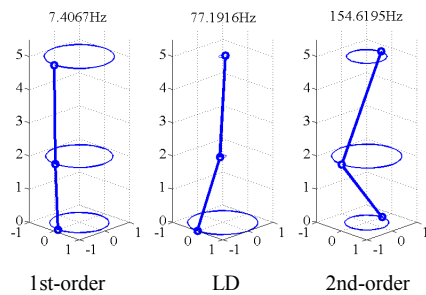


Fig. 6. Mode shapes (Rotating speed: 800 rps).

It can be seen from Figs. 3 and 4 that the lower damper mode and the second-order mode of the flywheel rotor will exchange for each other when the mode frequency of forward whirl of the conical mode of the flywheel rotor approaches the one of the lower damper with increasing speed. The vibration amplitude of the flywheel decreases in the lower damper mode and increases in the conical mode, while the vibration amplitude of the lower damper decreases in the conical mode. It is the zone of dual mode shapes when in the speed range 10 rps~100 rps. The exchange of modes is completed basically when the rotating speed exceeds 100 rps. Fig. 5 plots the mode shapes of the flywheel dynamic system when the rotating speed is 100 rps. The flywheel passes through the zones of cylindrical mode and dual modes in the spin test. Compared with conventional bearings, the stiffness of both elastic pivot and lower damper is very small, which makes their mode frequencies so close. The exchange of mode shapes occurring in a narrow frequency range is a new kind of dynamic characteristics produced by flexible damping support.

The speed for spin test is generally over 800 rps, at which the mode shapes of the system are as shown in Fig. 6. The mode frequency of the conical mode is much higher than 800 Hz so that it cannot be seen in the spin test. The lower damper mode shape still exists as the flywheel is fixed and the damper doing the lateral vibration, the first-order mode shape of the flywheel is still cylindrical mode.

### 3.3 Modal damping ratios

The modal damping ratio as the index to evaluate stability of the dynamic system also varies with the speed. Fig. 7 shows

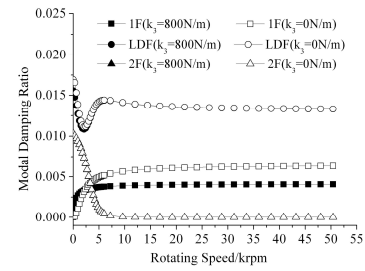


Fig. 7. The modal damping ratios of each mode.

that the modal damping ratios of the flywheel system varying with different speed with and without the auxiliary support.

As a result of the backward whirl being always stable and doesn't appear in the practice generally, only the characteristics of the forward whirl are discussed. For modes of forward whirl, when modal damping ratios are positive, the dynamics of the system is stable. The larger the ratio is, the better dynamic stability the system has.

Fig. 7 indicates the ratio of the first-order mode increases with increasing speed and exceeds 0.005. The ratio of the second-order mode decreases with increasing speed but is still positive, and it doesn't appear in the practice because it's always much higher than the rotating speed. The ratio of the lower damper mode increases with increasing speed and then decreases to 0.013. The auxiliary support mainly affects the first-order mode, and has little effect on the second-order mode and the lower damper mode. The stability of the first-order mode is enhanced when the upper support is removed in the test. To sum up, the dynamics of the flywheel system without the upper support is stable, and has very simple structure.

### 3.4 The lower damper parameters' influence on mode frequencies and modal damping ratios

For the high-speed composite flywheel that endures large centrifugal force, resin minor damages and fiber part breaks may produce non-ignorable disturbances and cause rotor-bearing system that has small modal damping ratios to natural whirl modes with low frequencies, which threatens flywheel life and structural strength seriously. The parameters of the lower damper should be adjusted to increase the modal damping of the rotor dynamic system and accelerate decaying the natural whirl.

Fig. 8(a) and (b) show the lower damper stiffness's influence on mode frequencies and modal damping ratios when the test speed is 800 rps. With increasing stiffness of the damper, the frequencies of the flywheel first-order mode and the lower damper mode increase slightly, which indicates the stiffness has a little effect on the pair of frequencies. However, the larger stiffness decreases the modal damping ratios of the flywheel first-order mode and the lower damper mode greatly. Therefore, the larger stiffness makes the stability of the system be worse. The smaller stiffness will lead to worse centering of

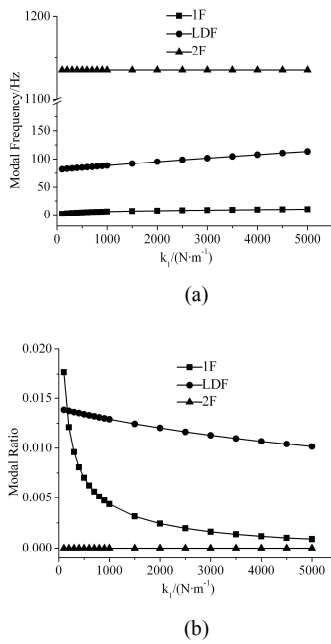


Fig. 8. The lower damper stiffness's influence.

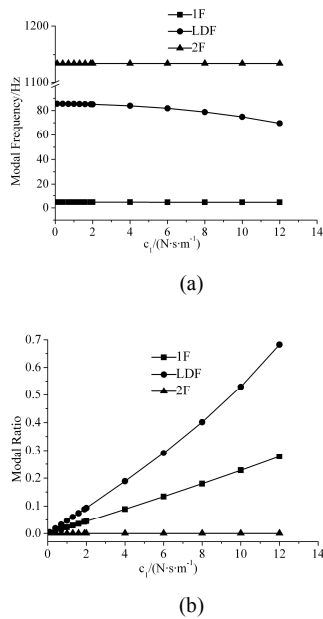


Fig. 9. The damping's influence.

rotor-bearing system. So the stiffness 500 N/m~2000 N/m is too small and not suggested.

Fig. 9(a) and (b) show the damping's influence on the modal frequencies and modal damping ratios when the test speed is 800 rps. The mode frequency of the lower damper decreases in some degree with increasing damping coefficient, which agrees with the basic theory of vibration. The damping coefficient has no effect on the frequencies of the first-order and second-order forward whirl of the flywheel. However, increasing damping coefficient can enhance the stability of the cylindrical mode of the flywheel and the lower damper mode effec-

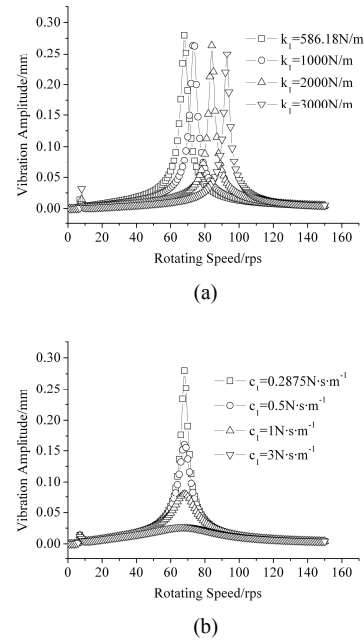


Fig. 10. Parameters' influence on  $|r_1|$ .

tively. The conical mode that always does not appear is not considered.

### 3.5 The lower damper parameters' influence on the amplitude-frequency responses of the forced vibration

In engineering practice, the flywheel rotor inevitably has mass unbalance. For the flat-shaped flywheel, most of the residual unbalance is at the flywheel rotor top. When the residual unbalance is  $0.1\text{g}\cdot\text{cm} \angle 0^\circ$ , the steady state unbalance responses can be calculated by Eq. (8), which can be used to estimate the vibration condition when the flywheel passes through the critical speeds. The eddy current sensors installed in the lower damper can measure the forced vibration responses of the damping body, so only the numerical result of the lower damper was presented. For  $k_3 = 800$  N/m,  $c_3 = 0$  N·s/m, amplitude-frequency response of the lower damper ( $|r_1|$ ) with different parameters is shown in Fig. 10(a) and (b). The larger stiffness increases the second critical speed greatly, which makes it difficult to pass the critical speed. The larger stiffness also leads to the larger vibration amplitude when passing the first critical speed. However, increasing damping coefficient can significantly suppress the amplitude of the vibration when the flywheel passes the two critical speeds and has little effect on the critical speeds of the system. It also can be seen the lower damper tends to be overdamped when  $c_1 > 3$  N·s/m. Thus, the rising stiffness of the lower damper neither enhances the stability of the flywheel system at high speed nor makes the flywheel rotor pass the critical speeds stably and easily. On the contrary, the rising damping coefficient of the lower damper not only enhances the stability of the flywheel system at high speed, but also makes the flywheel rotor pass the critical speeds stably and easily.

After the flywheel passes the two critical speeds, the amplitude of the vibration decreases rapidly, about 0.004 mm, which is the self-centering effect of super-critical rotor. From the above theoretical analysis and discussion, one perfect set of rotor dynamics parameters was selected for the high speed spin test system.

#### 4. Experimental verification

The major objectives of the experiments are: (a) to run the flywheel to high speed and find the appropriate dynamics parameters of the lower damper; (b) to measure the responses of the forced vibration of the lower damper; and (c) to verify the numerical simulation above.

We had built the spin test system as shown in Fig. 1 in our laboratory. The designed flywheel-bearing-damper system was installed in the vacuum chamber. The flywheel was statically indeterminate. An auxiliary support was needed to put on the upper end of the flywheel rotor to provide radial stiffness when its rotating speed rises. The auxiliary support was not removed until the flywheel rotor ran stably, and the flywheel would be tested at the high speed without the upper support. The sensor was installed at central section of the lower damper. The electrical signal by the preamplifier was input to the oscilloscope TDK2000. The amplitude-frequency curve of the damping body of the lower damper can be obtained by FFT analysis. The disk type motor is able to drive the flywheel rotor in continuous operation at the speed 120000 r/m for thousands of hours.

The dynamic parameters of the lower damper play an important role in dynamic stabilization of the flywheel system. The equivalent mass of the damper includes the mass of the damping body and the inertial of the viscosity of the damping substance in the damper. The equivalent damping coefficient is determined by the viscosity of the damping medium. The equivalent stiffness is determined by the three small stiffness springs. Absolute ethyl alcohol, absolute ethyl alcohol mixed with a little vacuum oil and vacuum oil were used as the damping medium, respectively. The responses of vibration were obtained by FFT analysis with the oscilloscope TDK2000 after exciting the damping body. Based on vibration theory of the single degree of freedom, the equivalent mass, the equivalent stiffness and the equivalent damping coefficient of the lower damper can be obtained.

When the damping medium was absolute ethyl alcohol, the damper was underdamped, the dynamic parameters measured were:  $m_1 = 0.0197$  kg,  $k_1 = 586.18$  N/m,  $c_1 = 0.2875$  N·s/m. When the damping medium was absolute ethyl alcohol mixed with a little vacuum oil, the damper was also underdamped. The dynamic parameters measured were:  $m_1 = 0.021$  kg,  $k_1 = 586.18$  N/m,  $c_1 = 0.484$  N·s/m. When the damping medium was vacuum oil, the damper was overdamped. In this case,  $m_{1\min} = 0.021$  kg. When the single degree of freedom had a critical damping,  $c_{1\min} = 2\sqrt{m_{1\min}k_1} = 7.0171$  N·s/m. Therefore,  $m_1 > 0.021$  kg,  $c_1 > 7.0171$  N·s/m, when the

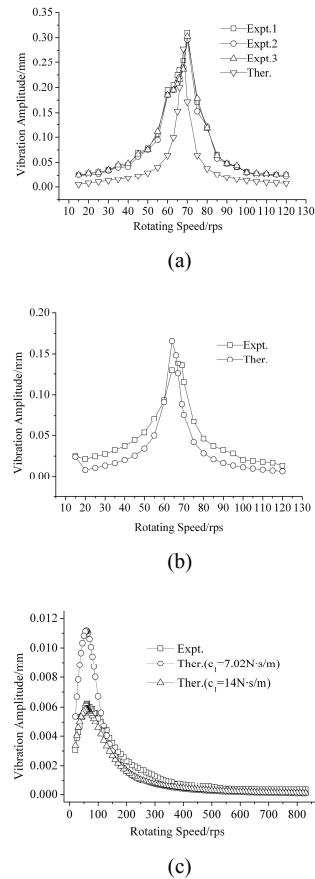


Fig. 11. Synchronous vibration of the lower damper.

damper was overdamped.

The disk motor and inverter had significant interference on the eddy current sensor, so the amplitude-frequency response was measured when the rotating speed was falling down as the motor was being turned off. Because there was no upper support, the flywheel dynamic system had only one critical speed, corresponding to the mode of the lower damper. Because the section diameter of the pivot is about 1.5 mm, it is difficult to carry out the dynamic balance of the flywheel. For the flat-shaped flywheel, most of the residual unbalance was at the flywheel rotor top. It was propounded that the residual unbalance can be calculated by Eqs. (5) and (8) using three different sets of dynamic parameters of the lower damper.

Three measurements were carried out when the absolute ethyl alcohol was used as the damping medium in the first spin test. Because of the violent vibration of the damping body, the maximum rotating speed was only 125 rps. The amplitude-frequency response was measured and recorded as shown in Fig. 11(a).

The critical speed measured was 70 rps; the corresponding theoretical result is 69 rps. When the residual unbalance is  $0.1 \text{ g}\cdot\text{cm} \angle 0^\circ$ , the theoretical amplitude of synchronous vibration is slightly smaller than the measured one.

Absolute ethyl alcohol mixed with a little vacuum oil as the damping medium was used in the second spin test. The maxi-

imum rotating speed was still 125 rps. The amplitude-frequency response was measured and recorded as shown in Fig. 11(b). The critical speed measured was 68 rps; the corresponding theoretical result is 65 rps. When the residual unbalance is  $0.1 \text{ g}\cdot\text{cm} \angle 0^\circ$ , the theoretical amplitude is slightly smaller than the measured one except when the flywheel passes the critical speed. Based on the tests above, the comparison between the calculated unbalance response and the experimental response indicates that the dynamic model is proper.

The rising damping coefficient of the lower damper enhances the stability of the flywheel system at high speed and suppresses the amplitude of vibration when the flywheel rotor passes the critical speeds, which is helpful for the reliable and durable operation of jewel bearing. The damping medium in the third spin test is vacuum oil, so the damper is overdamped. Then dynamic parameters are difficult to obtain by excitation. It is propounded that the equivalent mass  $m_1$  is 0.021 kg which is smaller than the real value. The equivalent damping coefficient is taken as 7.0171 N·s/m, which is the critical damping, so that the actual value of damping coefficient which is over damping is greater than 7.0171 N·s/m. The equivalent stiffness  $k_1$  is 586.18 N/m, which is determined by three springs. Based on the assumptions above, the theoretical value of the critical speed should be more than the measured one, and the theoretical amplitude of synchronous vibration of the lower damper should be also more than the measured one.

The vibration amplitude was much smaller than results of the previous two tests in the third spin test; the flywheel ran up to 830 rps steadily. Considering the limitation of the material strength used to manufacture the flywheel rotor, the higher speed spin test wasn't carried out. The amplitude-frequency response was measured and recorded as shown in Fig. 11(c). The critical speed measured was 56 rps, which is smaller than the theoretical result is 62 rps in the third spin test, because the equivalent mass of the overdamped damper is greater than 0.021 kg. The smaller mass used in the numerical simulation makes the higher theoretical result. The equivalent damping coefficient, which is corresponding to over damping, is larger than one, which is corresponding to critical damping. Therefore, the measured amplitude of synchronous vibration is smaller than the theoretical one, which is in agreement with Fig. 11(c). According to the measured amplitude of synchronous vibration, the equivalent damping coefficient 14 N·s/m can be conjectured from combining with numerical result.

In the process of speed reduction, the energy loss consists of the friction of flywheel and rare gas, the friction of the pivot-jewel bearing, and energy consumed by the lower damper. Assuming that kinetic energy of the flywheel is only consumed by the pivot-jewel bearing, the maximum average friction power was 1.2W.

The friction heat of the lubricating oil is conducted to the cooling system of the disk type motor through the housing of the damper. However, the conventional high speed bearings

usually require oil fog lubrication or oil jet lubrication, which has low efficiency and high cost. A number of spin tests were carried out when the damper was overdamped; the flywheel could run up to 830 rps steadily.

## 5. Conclusions

(1) The pivot-jewel bearing with small stiffness spring and squeeze film damper were used as the lower support of the flywheel spin test system. The auxiliary support at the top was not removed until the flywheel rotor passed the first critical speed, and the flywheel strength was tested at the high speed without the upper support. The super-critical rotor dynamics flywheel-bearing-damper system is simple, stable and efficient in structure.

(2) By means of the Lagrangian equation, a linear dynamics system with three-degrees of complex freedom was built to describe the free and forced vibrations of the flywheel rotor-bearing-damper system. The numerical simulation indicates that the dynamics of the flywheel system without the upper support is stable. The flexible pivot greatly reduces the critical speeds of the system and makes it easy for the flywheel to pass the two critical speeds that correspond to the zones of cylindrical mode and conical mode, respectively. The small stiffness of the support takes full advantage of the effect of self-centering of the high speed rotor. The exchange of mode shapes that occur in a narrow frequency range is a new kind of dynamic characteristic produced by flexible damping support. The rising damping coefficient of the lower damper not only enhances the stability of the flywheel system at high speed, but also helps the flywheel rotor pass the critical speeds stably and easily.

(3) The comparison between the calculated unbalance response and the experimental response indicates that the dynamic model is appropriate. When vacuum oil was used as the damping medium, the damper was overdamped. So the flywheel ran up to 50,000 r/min steadily. The equivalent damping coefficient 14 N·s/m and the real residual unbalance  $0.1 \text{ g}\cdot\text{cm}$  were estimated from combining experimental measurement with numerical result.

(4) Other tests indicated that the spin test system was suitable for the flywheel with mass between 0.5-2.0 kg. For larger flywheel test samples, the parameters of the flexible damping support (including pivot, spring and jewel bearing) can be designed through the theoretical model and analysis method discussed in this paper.

## Acknowledgment

This work was supported by the National Natural Science Foundation of China (Grant Number: 11075087).

## Nomenclature

$m_1$  : Mass of the spring squeeze film damper

$M$	: Mass of the flywheel rotor
$J_p$	: Polar moment inertia of the flywheel rotor
$J_d$	: Diameter moment inertia of the flywheel rotor
$l$	: Length of the flywheel rotor
$l_1$	: Length between mass center and its upper end
$l_2$	: Length between mass center and its lower end
$l_s$	: Length of the pivot
$k_1$	: Stiffness of the spring squeeze film damper
$k_2$	: Stiffness of the pivot
$k_3$	: Stiffness of the auxiliary support
$c_1$	: Damping coefficient of the squeeze film damper
$c_3$	: Damping coefficient of the auxiliary support
$x_1, y_1$	: Vibration of the spring squeeze film damper
$x_2, y_2$	: Vibration of the flywheel rotor bottom
$x_3, y_3$	: Vibration of the flywheel rotor top
$x_c, y_c$	: Mass centric coordinates
$r_1$	: Vibration of the spring squeeze film damper
$r_2$	: Vibration of the flywheel rotor bottom
$r_3$	: Vibration of the flywheel rotor top

## References

- [1] J. G. Bitterly, Flywheel technology: past, present, and 21st century projects, *IEEE Aerospace and Electronic Systems Magazine*, 13 (8) (1998) 13-16.
- [2] X. J. Dai, Z. P. Shen and H. G. Wei, On the vibration of rotor-bearing system with squeeze film damper in an energy storage flywheel, *International Journal of Mechanical Sciences*, 43 (11) (2001) 2525-2540.
- [3] L. Zhang and H. Zhang, Progress in study of flywheels made of composites, *Ordinance Material Science and Engineering*, 24 (5) (2001) 63-65.
- [4] D. A. Christopher and R. Beach, Flywheel technology development program for aerospace applications, *IEEE Aerospace and Electronic Systems Magazine*, 2 (1997) 602-608.
- [5] R. B. Schainker, Executive overview: energy storage options for a sustainable energy future, *IEEE Power Engineering Society General Meeting*, 2 (2004) 2309–2314.
- [6] B. Yang, Y. Makarov and J. Destees1, et al, On the use of energy storage technologies for regulation services in electric power systems with significant penetration of wind energy, *Electricity Market* (2008) 1-6.
- [7] R. Hebner and J. Beno and A. Walls, Flywheel batteries come around again, *IEEE Spectrum*, 39 (4) (2002) 46-51.
- [8] R. G. Lawrence, K. L. Craven and G. D. Nichols, Flywheel UPS, *IEEE Industry Applications Magazine*, 9 (3) (2003) 44-50.
- [9] H. S. Kyu, D. J. Kim and T. H. Sung, Optimum design of multi-ring composite flywheel rotor using a modified generalized plane strain assumption, *International Journal of Mechanical Sciences*, 43 (4) (2001) 993-1007.
- [10] F. Abdel-Hady, G. Baaklini and Y. Gowayed, et al. Manufacture and NDE of multi-direction composite flywheel rims. *Journal of Reinforced Plastics and Composites*, 24 (4) (2005) 413-421.
- [11] S. K. Ha, J. H. Kim and Y. H. Han, Design of a hybrid composite flywheel multi-rim rotor system using geometric scaling factors, *Journal of Composite Materials*, 42 (8) (2008) 771-785.
- [12] A. C. Arvin and C. E. Bakis. Optimal design of press-fitted filament wound composite flywheel rotors. *Composite Structures*, 72 (1) (2006) 47-57.
- [13] X. J. Dai, H. G. Wei and Z. P. Shen, Dynamics design and experiment study of the rotor-bearing system of a flywheel energy storage system, *Chinese Journal of Mechanical Engineering*, 39 (4) (2003) 97-101.
- [14] X. J. Dai, H. G. Wei and Z. P. Shen, Study on whirl modal damping of energy storage flywheel-bearing system, *Journal of Vibration Engineering*, 15 (1) (2001) 98-101.
- [15] X. J. Dai, C. L. Tang and S. Q. Yu, Measuring friction coefficient of the high speed pivot bearing in oil-bath lubrication by a varying load method, *Tribology*, 31 (2011) 7-11.
- [16] C. L. Tang and X. J. Dai. The analysis on anti-wear properties advantage of high speed improved pivot-jewel bearing, *Machine Design and Research*, 26 (5) (2010) 67-70.



**Changliang Tang** received the B.S. in Automation Engineering from Tsingtao University in 2008 and M.S. in Nuclear Science and Technology from Tsinghua University in 2010. He is currently a graduate student pursuing the Ph.D. degree of Engineering Physics Department at Tsinghua University. His research interests are rotor dynamics and bearing technology, structural strength and mechanics of composite materials.